Burger, R. M., Peisach, J., & Horwitz, S. B. (1982) *J. Biol. Chem. 257*, 8612–8614.
Giloni, L., Takeshita, M., Johnson, F., Iden, C., & Grollman, A. P. (1981) *J. Biol. Chem. 256*, 8608–8615.
Harris, G., Ator, M., & Stubbe, J. (1984) *Biochemistry 23*, 5214–5225.
Hoard, D. E., & Ott, P. G. (1965) *J. Am. Chem. Soc. 87*, 1785–1788.
Joyce, C. M., & Grindley, N. D. P. (1983) *Proc. Natl. Acad. Sci. U.S.A. 79*, 744–748.
Stubbe, J., Ackles, D., Sehgal, R., & Blakley, R. L. (1981) *J. Biol. Chem. 256*, 4843–4846.
von Sonntag, C., & Schulte-Frolinde, D. (1978) in *Effects of Ionizing Radiation on DNA* (Hütterman, J., Köhnlein, W., Teoule, R., & Bertinchamps, A. J., Eds.) pp 219–226, Springer-Verlag, New York.
Wu, J. C., Kozarich, J. W., & Stubbe, J. (1983) *J. Biol. Chem. 258*, 4694–4697.
Wu, J. C., Kozarich, J. W., & Stubbe, J. (1985) *Biochemistry* (preceding paper in this issue).

Structure of the Anthramycin–d(ATGCAT)$_2$ Adduct from One- and Two-Dimensional Proton NMR Experiments in Solution†

David E. Graves,‡ Michael P. Stone,§ and Thomas R. Krugh*
Department of Chemistry, University of Rochester, Rochester, New York 14627
Received December 28, 1984; Revised Manuscript Received June 19, 1985

ABSTRACT: One- and two-dimensional 400-MHz proton NMR experiments are used to examine the solution structure of the covalent adduct formed by the interaction of anthramycin methyl ether with the self-complementary deoxyoligonucleotide d(ATGCAT)$_2$. The concentration dependence of chemical shifts and nuclear Overhauser enhancement (NOE) experiments are utilized to assign the adenine H_2 protons within the minor groove for both free d(ATGCAT)$_2$ and the adduct. These studies demonstrate that one of the four adenine H_2 protons is in close proximity to the bound anthramycin and this results in its upfield shift of 0.3 ppm compared to the adenine H_2 protons of the free duplex. Effects of the covalent attachment of anthramycin to the d(ATGCAT)$_2$ duplex result in an increased shielding of selected deoxyribose protons located within the minor groove of the adduct, as demonstrated by two-dimensional autocorrelated (COSY) NMR techniques. Interactions between the protons of the covalently attached anthramycin and the d(ATGCAT)$_2$ duplex are determined by utilizing two-dimensional NOE (NOESY) techniques. Analysis of these data reveals NOE cross-peaks between the anthramycin methyl, H_6, and H_7 protons with specific deoxyoligonucleotide protons within the minor groove, thus allowing the orientation of the drug within the minor groove to be determined. Nonselective inversion recovery (T_1) relaxation experiments are used to probe the structural and dynamic properties of the anthramycin–d(ATGCAT)$_2$ adduct. These data suggest that the binding of anthramycin alters the correlation time of the d(ATGCAT)$_2$ duplex and stabilizes both of the internal A·T base pairs with respect to solvent exchange. The solution conformation of the anthramycin–d(ATGCAT)$_2$ adduct, as deduced from the NMR data, is in agreement with model-building studies [Hurley, L. H., & Petrusek, R. L. (1979) *Nature (London) 282*, 529–531; Petrusek, R. L., Anderson, G. L., Garner, T. F., Fannin, Q. L., Kaplan, D. J., Zimmer, S. G., & Hurley, L. H. (1981) *Biochemistry 20*, 1111–1119].

The antitumor activity of anthramycin (Figure 1A) has been attributed to its ability to interact with DNA resulting in the inhibition of the biosynthesis of nucleic acids (Kohn et al., 1968; Stefanovic, 1968; Horwitz et al., 1971; Glaubiger et al., 1974). The exact nature of this interaction with DNA has been the subject of numerous studies over the past several years. From these studies, anthramycin has been shown to form a labile covalent attachment to DNA spanning approximately three base pairs (Glaubiger et al., 1974; Kohn & Spears, 1970; Kohn et al., 1974). The stability of this bond is dependent upon the maintenance of the secondary structure of the DNA and is lost upon denaturation of the DNA by heating, by enzymatic digestion, or by lowering the pH to <7.0. Anthramycin is highly selective in binding to DNA, requiring the presence of both a double-strand DNA template and guanine (Hurley et al., 1979). This nonintercalative interaction results in the thermal stabilization of the duplex and is presumed to occur in the minor groove (Hurley & Petrusek, 1979; Petrusek et al., 1981).

Recently, nuclear magnetic resonance techniques were used to confirm the points of attachment of anthramycin to DNA (Graves et al., 1984). Analysis of ^{13}C NMR spectra demonstrated that the anthramycin forms a covalent linkage to the DNA at the C_{11} position. The site of attachment on the DNA was determined by using the self-complementary deoxyoligonucleotide d(ATGCAT)$_2$ as a DNA model. ^1H NMR studies confirmed the guanine NH_2 as the site of attachment to the DNA, consistent with the model proposed (Hurley & Petrusek, 1979; Petrusek et al., 1981). Upon formation of the adduct, a loss in the helical symmetry of the self-complementary deoxyoligoribonucleotide resulted in the doubling of the nucleotide resonances. The doubling, combined with superposition of anthramycin resonances, resulted in a complex spectrum that could not be unequivocally assigned, thus pre-

†This work was supported by National Cancer Institute Grants CA-35251 and CA-17865.
‡Present address: Department of Chemistry, University of Mississippi, University, MS 38677.
§Present address: Department of Chemistry, Vanderbilt University, Nashville, TN 37235.

0006-2960/85/0424-7573$01.50/0

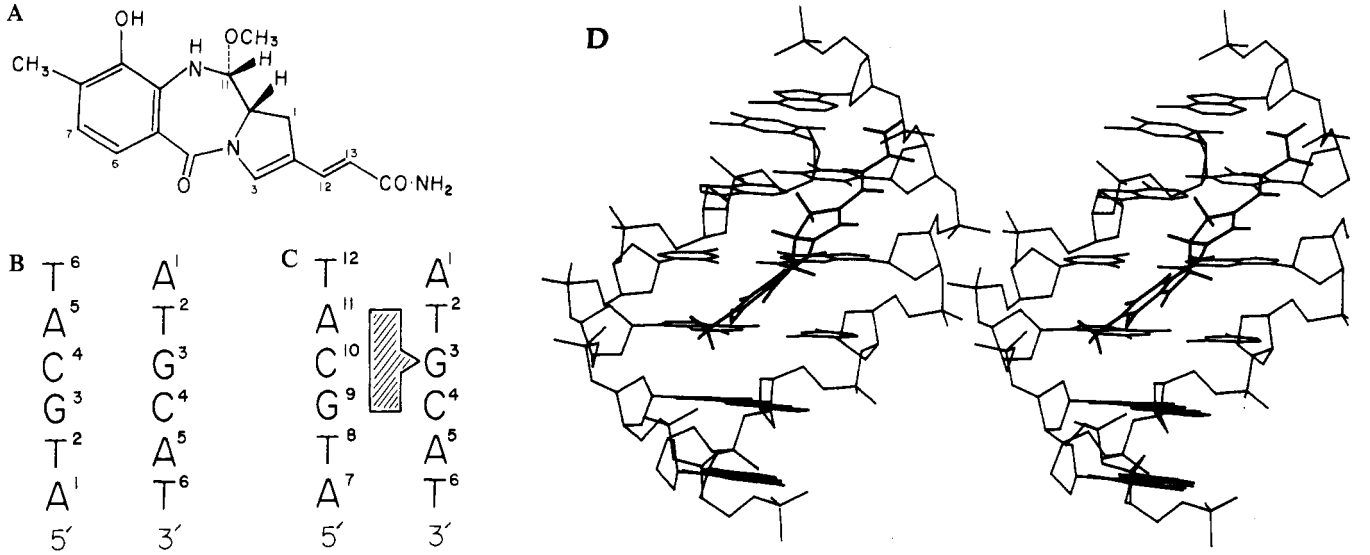

FIGURE 1: (A) Chemical structure and numbering scheme of anthramycin methyl ether. (B) Schematic representation of the numbering system for the symmetrical self-complementary d(ATGCAT)$_2$. (C) Schematic representation of the numbering system for the anthramycin–d(ATGCAT)$_2$ adduct. (D) Stereoview of the anthramycin–d(ATGCAT)$_2$ adduct, illustrating the orientation of the anthramycin moiety within the minor groove of the DNA duplex, based on B-DNA geometry and generously provided by Dr. Laurence H. Hurley. The anthramycin is attached covalently to the DNA via an aminal linkage between the C_{11} position and the guanine NH_2, spanning a three base pair region of the oligomer.

cluding an in-depth examination of the structural features of the anthramycin–DNA adduct.

We present in this paper a combination of one-dimensional nuclear Overhauser (NOE), two-dimensional NOE (NOESY), and two-dimensional autocorrelated (COSY) experiments to obtain definite assignments of the most important resonances in the spectrum of the anthramycin–d(ATGCAT)$_2$ adduct. These data provide insight into the structure and dynamics of the anthramycin–d(ATGCAT)$_2$ adduct in solution and serve as a paradigm for the study of ligands covalently attached to double-stranded DNA.

Experimental Procedures

Materials. Anthramycin methyl ether was generously supplied by Professor Laurence H. Hurley, Drug Dynamics Institute, University of Texas at Austin. The deoxyoligoribonucleotide d(ATGCAT)$_2$ (lot no. 689-64) was purchased from Pharmacia, P-L Biochemicals, Milwaukee, WI. Purity and authenticity of the hexamer were determined by high-performance liquid chromatography (HPLC) and ^{1}H NMR spectroscopy.

Sample Preparation. The anthramycin–d(ATGCAT)$_2$ adduct was prepared by dissolving ~5 mg of d(ATGCAT)$_2$ in 0.4 mL of buffer [10 mM sodium phosphate, 0.1 mM disodium ethylenediaminetetraacetate (Na_2EDTA), 100 mM sodium chloride, pH 7.0]. Crystalline anthramycin (~5 mg) was added to the hexamer solution, followed by vigorous stirring. The drug–hexanucleotide mixture was allowed to react for 48 h at 5 °C in the absence of light. At the end of 48 h, the solid anthramycin was removed by centrifugation, and the clear supernatant was extracted 5 times with buffer-saturated 1-butanol. After extraction of the "nonbound" drug, the stoichiometry of the resulting adduct was determined to be 2:1 (strand:drug) on the basis of extinction coefficients ϵ_{343} of 41 500 M^{-1} cm^{-1} per strand (Breslauer, 1981) and drug–DNA adduct ϵ_{343} of 31 800 M^{-1} cm^{-1}. The absorbance at 260 nm of the adduct was corrected by subtracting 20% of the 343-nm absorbance (Kohn & Spears, 1970).

NMR Experimental Parameters. All experiments were performed on a Bruker WH-400 spectrometer operating at a proton frequency of 400 MHz. The samples in D_2O were exchanged 3 times by lyophilization. The H_2O samples contained 10% D_2O as a spectrometer lock compound. Samples were maintained at 5 °C and purged with dry nitrogen for 30 min prior to capping. Chemical shifts were referenced internally to 3-(trimethylsilyl)propionate (TSP). Temperature was controlled within 0.5 °C and was measured by using methanol or ethylene glycol as a reference compound. Spectra for the samples dissolved in H_2O were obtained by using a time-shared hard pulse (Graves et al., 1984; Haasnoot, 1983; Haasnoot & Hilbers, 1983).

(*a*) *One-Dimensional NOE Experiments.* Transient peak saturation was accomplished by gating the decoupler on prior to pulsing the sample. Typical irradiation times were 250–500 ms for samples in D_2O (to minimize spin diffusion) and 100–500 ms for H_2O samples. The power level was 0.2 W, 40 dB, for D_2O samples, and 0.2 W, 30 dB, for H_2O samples. Spectra were acquired into 16K (complex) points by using quadrature detection, and an exponential weighting was applied prior to transformation. Recycle delays of 1 (H_2O) and 4 s (D_2O) were used. Difference spectra were obtained by subtraction of a control free induction decay (FID) in which the decoupler was set off-resonance.

(*b*) *Two-Dimensional NOESY Experiments.* Data were obtained by using the standard $(90°-t_1-90°-\tau_m-90°)_n$ pulse sequence and consisted of 256 t_1 values, each having 2K complex points. Typical data sets contained 16 acquisitions and 4 dummy scans for each FID; some contained 32 acquisitions per FID. Values for the recycle delay and the mixing time (τ_m) were 6 s and 600 ms, respectively. The mixing time was randomly varied by 20% to reduce cross-peaks arising from scalar coupling. The residual HDO peak was suppressed by homogated decoupling, gated off during the acquisition period. The data were zero-filled in the t_1 dimension to 1K, to yield a 1K by 1K data matrix, with digital resolution of 3.9 Hz/point. Sine bell apodization was used in both dimensions. The data were symmetrized; the resulting contour plot was compared to a nonsymmetrized contour plot to check for artifacts.

(*c*) *Two-Dimensional COSY Experiments.* Data were obtained by using a $(90°-t_1-90°)_n$ pulse sequence and consisted of 256 t_1 values, each having 2K complex points. Each FID contained 32 acquisitions; 4 dummy scans were used. Qua-

drature detection was used in both dimensions. The data were zero-filled in t_1 to 1K. Sine bell apodization was used in both dimensions, and symmetrization was performed on the data. The recycle delay was 4 s. The residual HDO peak was suppressed by homogated decoupling, which was gated off during acquisition.

(*d*) *T_1 Experiments.* These experiments utilized the standard nonselective 180°–τ–90° pulse sequence. The recycle delay was 10 s for the samples in D_2O and 1 s for the samples in H_2O. The FID was digitized into 16K (complex) points using quadrature detection, yielding a digital resolution of 0.5 Hz/point. An exponential weighting of 1 was applied to the data prior to Fourier transformation. A range of 0–20 s was used for values of τ for the D_2O samples, and values of 0–4 s were used for the H_2O samples. Generally, 32 scans were collected for each τ value, along with 4 dummy scans. T_1 values were determined from plots of the peak intensity as a function of the τ values.

Results

The numbering schemes of the self-complementary d-(ATGCAT)$_2$ duplex and the anthramycin–d(ATGCAT)$_2$ adduct are presented in parts B and C, respectively, of Figure 1. The free oligonucleotide contains a 2-fold axis of symmetry (Figure 1B), resulting in equivalence of the corresponding base protons between both DNA strands (Patel & Tonelli, 1975). The covalent bond formed by the anthramycin–d(ATGCAT)$_2$ adduct has been characterized as an aminal linkage of the anthramycin C_{11} and the 2-amino group of guanine (Graves et al., 1984). As shown in Figure 1C, the anthramycin is depicted as binding at G^3, spanning a 3 base pair region, and is in close proximity to the T^2·A^{11}, G^3·C^{10}, C^4·G^9, and A^5·T^8 base pairs. A more detailed examination of this binding model is provided by the stereo drawing in Figure 1D, illustrating the covalent attachment of anthramycin to one of the central guanines residing within the minor groove of the d(ATGCAT)$_2$ duplex.

Concentration Dependence of the Anthramycin–d-(ATGCAT)$_2$ Chemical Shifts. The loss of the helical symmetry of the deoxyoligonucleotide in the adduct is illustrated by the doubling of the resonances in the proton NMR spectra shown in Figure 2A. As the strand concentration of the adduct is increased from 0.5 to 5 mM, the appearance of the spectrum changes, due to the enhanced shielding effects resulting from the more favorable stacking interactions at the higher concentrations (Young & Krugh, 1975). In this range of concentrations, the adenine H_8 protons undergo ~0.02 ppm downfield shifts while the guanine H_8 resonances exhibit very little change. In contrast, the adenine H_2 protons (labeled a–d in Figure 2) demonstrate the largest chemical shift change as a function of the strand concentration. This finding is consistent with the general observation that for oligonucleotides, the chemical shift of adenine H_2 protons is often sensitive to stacking interactions (Lee & Tinoco, 1980; Neumann et al., 1982). The data in Figure 2B suggest that the resonances labeled a and b ($\Delta\delta > 0.1$ ppm) arise from the terminal adenine H_2 protons (A^1 and A^7), while resonances c and d ($\Delta\delta < 0.1$ ppm) are from the internal adenine H_2 protons (A^5 and A^{11}), since the effects of concentration should be greatest at the terminal positions where base pair fraying and intramolecular aggregation effects must be considered. However, assignments for adenine H_2 protons are often ambiguous due to the relatively isolated location of these protons in the minor groove of the duplex.

Assignment of the Individual Adenine H_2 Protons of d-(ATGCAT)$_2$ and the Anthramycin–d(ATGCAT)$_2$ Adduct.

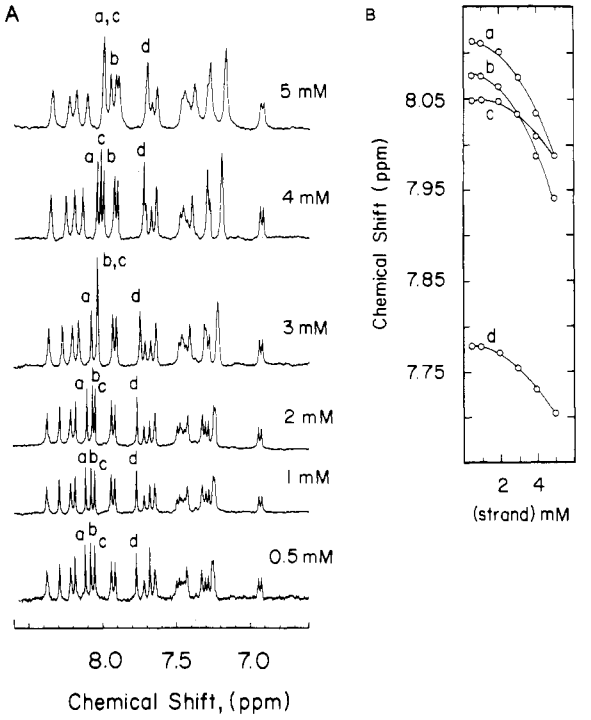

FIGURE 2: (A) 400-MHz proton NMR spectrum of the anthramycin–d(ATGCAT)$_2$ adduct in the 6.5–8.5 ppm range as a function of concentration. Spectra were recorded in D_2O at 15 °C. (B) Plot of the concentration dependence of the chemical shifts of the adenine H_2 protons from the terminal base pairs (labeled a and b) and the internal base pairs (labeled c and d).

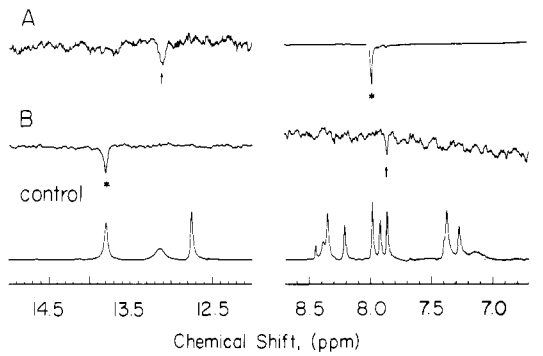

FIGURE 3: Assignment of the adenine H_2 protons in the self-complementary duplex, d(ATGCAT)$_2$, based on NOE connectivity peaks arising between selected imino and adenine H_2 resonances. Difference spectrum A corresponds to the irradiation of the adenine H_2 resonance at 8.0 ppm (*) resulting in the observation of an NOE connectivity peak at 13.2 ppm (designated by the arrow) corresponding to the terminal A·T imino resonance. Difference spectrum B shows that irradiation of the internal A·T imino resonance at 13.8 ppm (*) results in the observation of a negative connectivity peak corresponding to the upfield adenine H_2 proton at 7.87 ppm (shown by the arrow).

The data presented in Figures 3–5 provide a quantitative approach for determining the unequivocal assignments of the adenine H_2 resonances for both the unmodified and modified deoxyoligonucleotide duplexes. These results are based upon the observation of NOE connectivities between the adenine H_2 protons and their corresponding A·T imino protons (Weiss et al., 1984; Chou et al., 1983). The unequivocal identification of the adenine H_2 protons relies on the correct assignment of the imino resonances. The imino resonances of the d-(ATGCAT)$_2$ duplex were securely assigned by Patel (1974) and Hilbers & Patel (1975) on the basis of the sequential melting of the imino resonances at increasing temperatures. These imino proton assignments may be used to assign the adenine H_2 protons. In Figure 3A, irradiation of the adenine

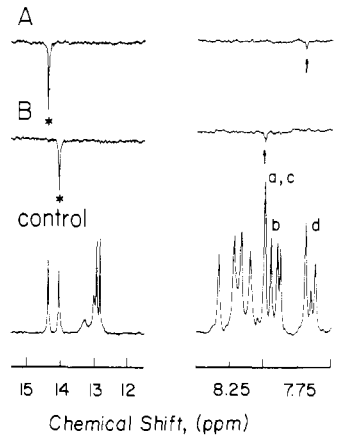

FIGURE 4: NOE difference spectra of the anthramycin–d(ATGCAT)$_2$ adduct at 15 °C in H_2O solution. The imino resonances were irradiated for 0.5 s prior to the observation pulse. (A) Difference spectrum resulting from irradiation of the internal A·T imino proton at 14.38 ppm (designated by *) with the observation of a negative NOE at 7.69 ppm (resonance d). (B) Difference spectrum resulting from irradiation of the internal A·T imino proton resonance at 14.06 ppm (designated by *) with the observation of a negative NOE at 7.98 ppm (resonances a and c).

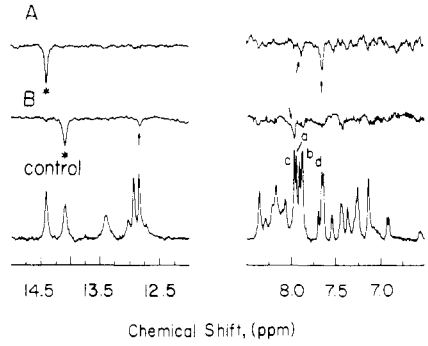

FIGURE 5: NOE difference spectra as in Figure 4 except the spectra were recorded at 5 °C. The NOEs shown by the arrows in this figure and in Figure 4 provide the unequivocal assignments of the adenine H_2 resonances, as described in the text. The imino resonances were irradiated for 0.55 s prior to the observation pulse.

H_2 resonance located at 8.0 ppm gives rise to an NOE at 13.2 ppm, the A^1·T^6 imino resonance, thus identifying this adenine H_2 resonance as the terminal A^1H_2 proton. Irradiation of the internal A^5·T^2 imino proton, shown in Figure 3B, results in the observation of an NOE at 7.87 ppm, corresponding to the internal A^5H_2 proton. These NOE data indicate that the previous assignments for the adenine H_2 resonances of d-(ATGCAT)$_2$ based on the temperature dependence of the H_2 chemical shifts (Patel, 1975) are incorrect and the earlier assignments should be reversed.

Utilization of the d(ATGCAT)$_2$ imino proton assignments of Patel (1974), along with comparisons of their melting properties (i.e., fraying) with those of the anthramycin–d-(ATGCAT)$_2$ adduct, has allowed us to assign the terminal, internal, and central imino resonances of the adduct (Graves et al., 1984).

Previous assignments for the adenine H_2 resonances in the anthramycin–d(ATGCAT)$_2$ adduct were considered tentative (Graves et al., 1984). However, a combination of the NOE connectivities between the adenine H_2 and the imino protons along with an analysis of the temperature dependence of the chemical shifts as discussed above provides the unequivocal assignments for all four adenine H_2 protons and four of the six imino resonances. In Figure 4, the imino resonances at 14.38 and 14.06 ppm originate from the internal A^{11}·T^2 and A^5·T^8 base pairs. Saturation of the resonance at 14.38 ppm (Figure 4A) results in the observation of a negative NOE at 7.69 ppm, indicating that an internal adenine H_2 proton (designated as signal d) is associated with this A·T base pair. This adenine H_2 resonance exhibits a marked upfield shift in contrast to the other three adenine H_2 protons, indicative of shielding, which results from its close contact with the bound anthramycin. Analyses of Corey–Pauling–Koltun (CPK) models and the stereo drawing (Figure 1D) of the anthramycin–deoxyoligonucleotide adduct reveal that the $A^{11}H_2$ proton is in closest proximity to the anthramycin. Thus, we assign the adenine H_2 resonance at 7.69 ppm to the A^{11} nucleotide and the imino resonance located at 14.38 ppm to the A^{11}·T^2 base pair. This assignment is substantiated by NOE experiments, which will be discussed later.

Saturation of the internal A·T imino resonance located at 14.06 ppm (Figure 4B) results in the observation of an NOE at 7.98 ppm, corresponding to one of the superimposed adenine H_2 protons (designated as resonances a and c). Since resonance d is assigned to the $A^{11}H_2$ proton, the remaining internal adenine H_2 (A^5H_2) must be either resonance a or resonance c. This assignment is confirmed by inspection of Figure 2, which demonstrates the concentration dependence of the ^1H spectrum, allowing resonances a and c to be assigned as a terminal proton and the A^5H_2 proton, respectively. These assignments are substantiated by NOE experiments at 5 °C where all four adenine H_2 protons are observed as individual resonances, as shown in Figure 5. In Figure 5A, two NOEs are observed upon irradiation of the A^{11}·T^2 imino proton; one corresponds to peak d and the other, a less intense NOE observed at 7.88 ppm, results in the assignment of the resonance labeled a as the terminal A^1H_2 proton. Through elimination, resonance b can now be assigned as the terminal A^7H_2 proton.

Similarly, at 5 °C, irradiation of the A^5·T^8 internal imino resonance (Figure 5B) results in the observation of a pair of NOEs. One NOE is observed at 7.97 ppm, corresponding to the A^5H_2 proton, and a second NOE is observed in the imino region at 12.84 ppm, allowing this imino resonance to be assigned to the C^4·G^9 base pair. Again, by elimination, the remaining G·C imino resonance at 12.94 ppm is assigned to the G^3·C^{10} base pair. From these experiments, only the terminal A·T imino resonances at 13.0 and 13.25 ppm remain unassigned.

Assignment of the Deoxyribose Protons in d(ATGCAT)$_2$ and Anthramycin–d(ATGCAT)$_2$. The deoxyribose assignments may in principle be determined from analysis of two-dimensional NOESY and COSY data. NOE cross-peaks between the pyrimidine H_6 or purine H_8 proton and the $H_{1'}$ proton of the same nucleotide unit and the $H_{1'}$ proton of the adjacent 5′ nucleotide unit are characteristically observed for B-DNA; the deoxyribose spin systems can be separated in the COSY spectrum (Hare et al., 1983; Haasnoot et al., 1983; Feigon et al., 1983). However, strong cross-peaks were not observed in the NOESY spectra for the d(ATGCAT)$_2$ duplex nor for the anthramycin–d(ATGCAT)$_2$ adduct, at 15 °C. In the case of free d(ATGCAT)$_2$, this was undoubtedly due to the relatively low T_m of the duplex, in which substantial fraying, particularly of the terminal base pairs, occurs at 15 °C (Patel, 1974). The d(ATGCAT)$_2$ deoxyribose protons can be identified from the COSY and partial NOESY data (a series of COSY spectra were run at various temperatures aiding in the assignment procedure); however, it was not possible to make unequivocal assignments for all of the anthramycin–d(ATGCAT)$_2$ deoxyribose protons. Twelve in-

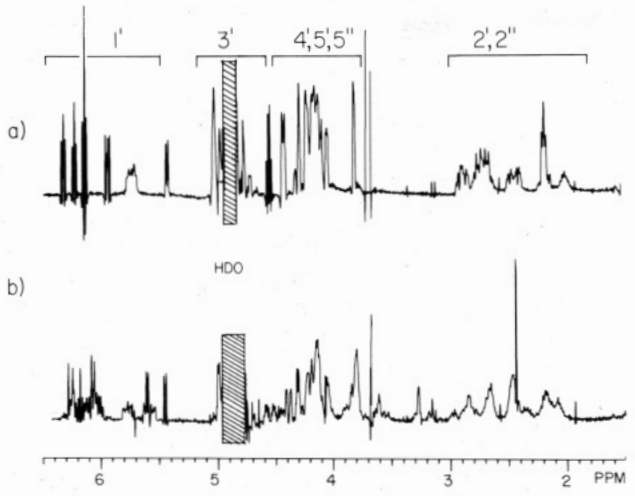

FIGURE 6: The deoxyribose region of the ^{1}H NMR spectrum of (a) d(ATGCAT)$_2$ and (b) the anthramycin–d(ATGCAT)$_2$ adduct. The spectra were recorded in D_2O at 15 °C. Resolution was enhanced by using a Gaussian multiplication function.

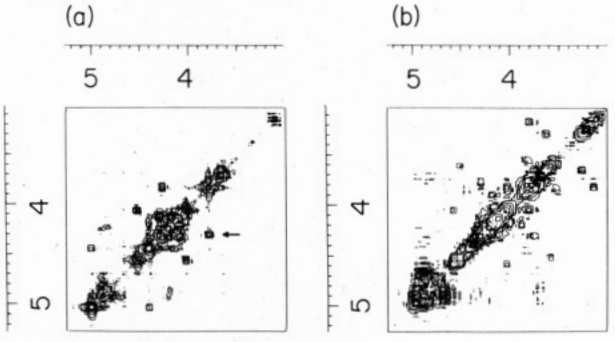

FIGURE 7: COSY spectra illustrating the deoxyribose $H_{3'}$, $H_{4'}$, $H_{5'}$, and $H_{5''}$ protons of (A) d(ATGCAT)$_2$ and (B) the anthramycin–d(ATGCAT)$_2$ adduct. In the spectrum of the free duplex (A), there are no cross-peaks upfield from 3.8 ppm. The arrow indicates the cross-peak between the $A^1H_{4'}$ and the $A^1H_{5',5''}$.

dividual spin systems are observed for the deoxyoligonucleotide adduct as a result of the loss of the 2-fold axis of symmetry upon binding the anthramycin.

Inspection of the one-dimensional NMR data shown in Figure 6 reveals that the covalent attachment of anthramycin results in marked chemical shift changes for several of the sugar proton resonances. The $G^3H_{1'}$ resonance is observed at 5.91 ppm for the free duplex (Figure 6a); in the adduct, neither $G^3H_{1'}$ nor $G^9H_{1'}$ is observed at this value (Figure 6b). Also, note the separation of the cytosine H_5 signals into two distinct doublets located at 5.4 and 5.6 ppm in Figure 6b. Large changes are also observed in the $H_{4'}$ and $H_{5',5''}$ region of the spectrum. In general, the chemical shifts of these protons are more dispersed for the anthramycin adduct than for the free hexamer duplex. In the free duplex, the $A^1H_{5'}$ and $A^1H_{5''}$ peaks are observed near 3.8 ppm (Figure 6a) and are the furthest upfield of the $H_{4'}$, $H_{5'}$, and $H_{5''}$ protons. Upon binding anthramycin, signals are observed at higher field (Figure 6b). This effect is clearly observed in Figure 7, where the COSY spectrum of the free hexamer is compared to that of the adduct. The location of the $A^1H_{4'}$–$A^1H_{5',5''}$ cross-peak (3.8, 4.3 ppm) is denoted by the arrow in Figure 7a. For d(ATGCAT)$_2$, no $H_{4'}$ or $H_{5',5''}$ cross-peaks are observed upfield of this value. However, Figure 7b demonstrates the presence of three distinct cross-peaks, which we assign to $H_{4'}$, $H_{5'}$, and $H_{5''}$ resonances that have shifted upfield upon addition of anthramycin. We assert that this effect is due to the close proximity of these protons above the aromatic ring of the anthramycin, as is

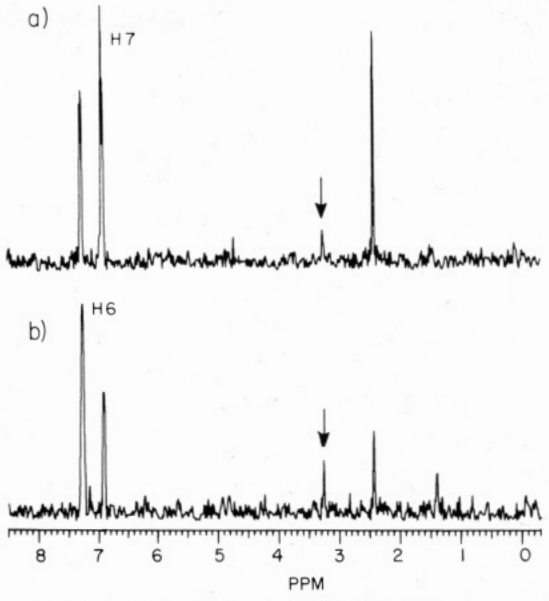

FIGURE 8: Cross-sectional plots from the NOESY spectrum of anthramycin–d(ATGCAT)$_2$. The cross-peaks denoted by the arrows arise from interaction between the anthramycin H_7 and H_6 protons with deoxyribose protons, which the COSY spectrum indicates are $H_{4'}$, $H_{5'}$, or $H_{5''}$ protons. The cross-peak observed at 2.4 ppm results from relaxation with the anthramycin methyl group. The peak at 1.4 ppm in spectrum b results from relaxation between a thymine methyl group and a thymine H_6 proton.

predicted by inspection of a CPK model of the adduct (Hurley et al., 1979) and the computer-generated structure shown in Figure 1D.

NOE Connectivities of the Anthramycin–d(ATGCAT)$_2$ Adduct. In an effort to determine the exact orientation of the drug relative to the deoxyoligonucleotide duplex, two-dimensional (2D) NOESY experiments were utilized, based upon the following rationale. Attachment of the anthramycin through the C_{11} position via an aminal linkage to the guanine NH_2 position should result in the association of the drug with the minor groove of the duplex. Thus, interactions between the protons of the bound anthramycin and DNA protons in the minor groove (i.e., the internal adenine H_2 protons and several deoxyribose protons) might be observed as NOE cross-peaks in the NOESY spectrum.

Figures 8 and 9 illustrate a cross-sectional representation and contour plot demonstrating NOE connectivities of the aromatic region of the anthramycin–d(ATGCAT)$_2$ spectrum. Several NOE connectivity peaks are observed in Figure 9, most resulting from dipole–dipole relaxation between the DNA protons. However, several cross-peaks resulting from anthramycin–DNA interactions are present and reveal key information concerning the structural properties of the anthramycin–d(ATGCAT)$_2$ adduct. Inspection of Figure 8, which is a cross-sectional representation through the anthramycin H_6 and H_7 protons, provides an indication of the signal-to-noise ratio of the NOESY data. In Figure 9, several of the cross-peaks enclosed by the box labeled A arise from dipolar interactions between the deoxyribose $H_{1'}$ protons and the purine H_8 and pyrimidine H_6 protons. As was previously discussed, these cross-peaks are characteristically seen for DNA in the B conformation and provide crucial information required to unequivocally assign the deoxyoligonucleotide protons. However, in the anthramycin–d(ATGCAT)$_2$ adduct, complete sets of these cross-peaks are not observed, thus precluding the unequivocal assignments of the deoxyribose protons. Four cross-peaks are observed connecting the cytosine H_5 doublets at 5.4 and 5.6 ppm with the corresponding cytosine

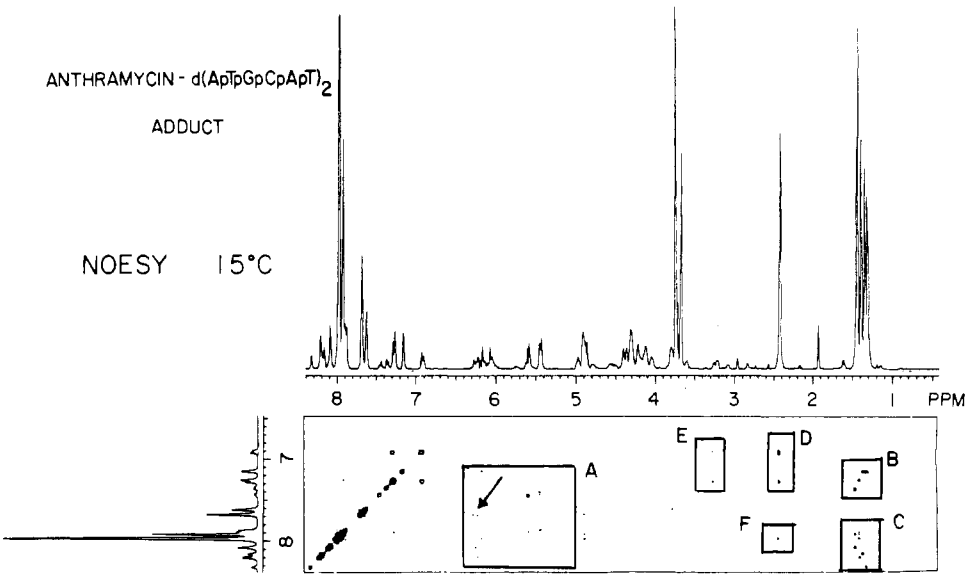

FIGURE 9: Expansion of the NOESY spectrum of the anthramycin–d(ATGCAT)$_2$ adduct illustrating the NOE connectivities between selected anthramycin and deoxyoligoribonucleotide protons. Cross-peaks in box A arise from connectivities between deoxyribose $H_{1'}$ and purine H_8, pyrimidine H_6. Those in box B arise from connectivities between thymine CH_3 and H_6 protons. Box C indicates thymine methyl–purine H_8 interactions. Box D shows cross-peaks between the anthramycin methyl and H_6 and H_7 protons. Anthramycin–d(ATGCAT)$_2$ interactions are observed in box E, arising from anthramycin H_6 and H_7 and deoxyribose $H_{4'}$, $H_{5'}$, or $H_{5''}$ protons. Cross-peaks arising between adenine H_2 and anthramycin protons are shown in box F, between the anthramycin methyl and the A^3H_2 proton. Additionally, the arrow in box A points to a possible cross-peak between the $A^{11}H_2$ and the anthramycin H_{13} protons.

H_6 doublets and also with the 5′ neighboring guanine H_8 protons. The cross-peaks denoted by the arrow in box A may arise from an interaction between the $A^{11}H_2$ and the anthramycin H_{13}. However, due to the overlap of the $A^{11}H_2$ and anthramycin H_{12} resonances and the coupling of the H_{12}–H_{13} protons it is speculative to regard this cross-peak as an anthramycin–DNA interaction.

The strong NOESY cross-peaks seen in boxes B and C arise from dipolar relaxations involving the four nonequivalent thymine methyl groups. In box B, strong cross-peaks are observed between the thymine methyl and the adjacent thymine H_6 protons. Cross-peaks observed in box C reflect relaxations involving these thymine methyls with the neighboring base pairs, mediated by "vertical" interactions in the major groove of the duplex. When the d(ATGCAT)$_2$ duplex is in the B form, the thymine methyls are in close proximity to the purine H_8 protons of the 5′ neighboring adenines (Feigon et al., 1983). The presence of these cross-peaks in the NOESY spectrum suggests that the binding of anthramycin does not induce large changes in the base-stacking properties of the duplex.

The two cross-peaks in box D arise from relaxation between the anthramycin methyl and the anthramycin H_6 and H_7 protons. This is more clearly illustrated in Figure 8, with the cross-sectional representation. In Figure 8a, a strong NOE at 2.4 ppm is observed between the anthramycin H_7 and the anthramycin methyl. A weaker NOE is observed in Figure 8b between the anthramycin H_6 and the anthramycin methyl; this may be due to spin diffusion effects resulting in a second-order NOE.

Cross-peaks arising from interactions between the anthramycin and the deoxyoligonucleotide are observed in boxes E and F of Figure 9. The cross-peaks in box E are also observed in Figure 8, denoted by the arrows at 3.25 ppm. From comparison of Figures 8 and 9 with Figure 7, we assign the NOE at 3.25 ppm to relaxation between the anthramycin H_6 and H_7 protons and deoxyribose $H_{4'}$, $H_{5'}$, or $H_{5''}$ protons, which are shifted upfield due to the presence of the drug. Inspection of molecular models indicates that the $A^{11}H_{5',5''}$ group would be in closest proximity to the anthramycin H_6 and H_7 within the minor groove.

The strong anthramycin–DNA cross-peak observed in box F of Figure 9 is indicative of the interaction between the anthramycin methyl and an adenine H_2 proton. Inspection of Figure 2 reveals that the A^5H_2 and A^1H_2 resonances are superimposed at 8 ppm at this sample concentration. However, the binding models of Hurley & Petrusek (1979), Mostad et al. (1978), and Petrusek et al. (1981) are consistent only with the observation of an NOE between the anthramycin methyl group and the A^5H_2 proton. The observation of this cross-peak provides evidence that the anthramycin is oriented within the minor groove such that the methyl group is close to A^5H_2.

Nonselective T_1 Experiments on d(ATGCAT)$_2$ and the Anthramycin–d(ATGCAT)$_2$ Adduct. The spin–lattice relaxation times (T_1) for the nonexchangeable aromatic protons in the 6.5–8.5 ppm range for d(ATGCAT)$_2$ and the anthramycin–d(ATGCAT)$_2$ adduct were compared with nonselective inversion recovery experiments in D_2O at 15 °C. The relaxation times and chemical shifts are tabulated in Table I.

For the d(ATGCAT)$_2$ duplex, the adenine H_2 protons exhibit the longest T_1 values (~4 s), more than twice the T_1 values of the other base protons of the deoxyoligonucleotide, which range from 1.1 to 1.4 s. These findings are qualitatively consistent with those of Patel & Tonelli (1975), with the values reported here being longer, as would be predicted due to the frequency dependence of T_1 when the product $\omega\tau_c$ is greater than 1. Examination of the data for the anthramycin–d(ATGCAT)$_2$ adduct reveals that, with the exception of the adenine H_2 protons, the base protons exhibit T_1 values that are 1.5–2 times larger than the relaxation times of the corresponding base protons of free hexamer. The adenine H_2 protons of the anthramycin–deoxyoligonucleotide adduct exhibit T_1 values ranging from 2.5 to 3.6 s with the $A^{11}H_2$ proton demonstrating the shortest T_1 of 2.5 s. The spin–lattice relaxation values for the adenine H_2 protons are of particular interest because of their relatively isolated location within the minor groove of the duplex; the binding of anthramycin in the minor groove should provide a strong source of dipolar re-

Table I: Chemical Shifts and T_1 Relaxation Values Obtained from Nonselective Inversion Recovery Experiments for the Nonexchangeable Base Protons of d(ATGCAT)$_2$ and the Anthramycin–d(ATGCAT)$_2$ Adduct (Both 5 mM) at 15 °C in D_2O[a]

d(ATGCAT)$_2$			anthramycin–d(ATGCAT)$_2$		
resonance	ppm	T_1 (s)	resonance	ppm	T_1 (s)
A^5H_8	8.33	1.4	AH_8	8.33	2.0
			AH_8	8.21	1.9
A^1H_8	8.18	1.4	AH_8	8.17	1.9
			AH_8	8.09	2.0
A^1H_2	7.97	4.0	A^1H_2	7.98	<4[b]
			A^7H_2	7.94	3.1
A^5H_2	7.87	4.0	A^5H_2	7.98	<4[b]
			$A^{11}H_2$	7.69	2.5
G^3H_8	7.92	1.4	GH_8	7.90	2.0
			GH_8	7.88	2.2
C^4H_6	7.39	1.1	CH_6	7.45	1.9
			CH_6	7.42	1.9
T^2H_6	7.36	1.1	TH_6	7.37	1.9
			TH_6	7.27	2.0
T^6H_6	7.28	1.2	TH_6	7.17	2.0
			TH_6	7.17	2.0

[a] For the adduct, absolute assignments have been determined for the adenine H_2 protons. [b] The resonances for A^1H_2 and A^5H_2 are superimposed at this concentration. Plots of the data are nonlinear, indicating that these two protons have different values of T_1, both less than 4 s.

laxation to adenine H_2 protons adjacent to anthramycin protons. The $A^{11}H_2$ resonance moves upfield upon adduct formation and is in close proximity to the acrylamide chain of the bound anthramycin in the CPK model of Petrusek et al. (1981). The 3.1-s T_1 value observed for A^5H_2 may result from the dipolar relaxation of this proton with the anthramycin methyl; an NOE between these two groups was shown in Figure 9. The terminal adenine H_2 protons, A^1H_2 and A^7H_2, are a greater distance from the anthramycin; however, they still relax more rapidly than the A^1H_2 in the free duplex. The lengthening of the T_1 relaxation times of the base protons (with the exception of the adenine H_2 protons as discussed above) indicates that the tumbling motions of the anthramycin–d(ATGCAT)$_2$ adduct are significantly altered, in comparison to the free deoxyoligonucleotide duplex. At 400 MHz, a minimum value of T_1 as a function of the molecular correlation time is expected for motion with a correlation time of $\sim$1 ns ($\omega\tau_c = 1$). Measured values of overall correlation times for short DNA duplexes are on the order of 5–10 ns (Feigon et al., 1983; Borer et al., 1984).

The nonselective inversion recovery of the imino resonances for d(ATGCAT)$_2$ and the anthramycin–d(ATGCAT)$_2$ adduct is illustrated in Figure 10. For the free oligomer (Figure 10A), we observe T_1 values in the range of 30 ms. Upon formation of the covalent anthramycin adduct, the T_1 relaxation values for the G·C and terminal A·T imino protons appear qualitatively similar to those of the free d(ATGCAT)$_2$ duplex (Figure 10B). However, T_1 values for both internal A·T imino protons of the adduct have increased in comparison to those of the free duplex, with the A^{11}·T^2 imino proton (14.38 ppm) exhibiting the longest T_1 value. This imino proton also exhibits the highest T_m (Graves et al., 1984) of the four A·T base pair imino protons in the anthramycin adduct.

Discussion

In previous studies, questions regarding the orientation of the anthramycin–deoxyoligonucleotide adduct were not fully addressed, in part because the complex proton NMR spectrum of the adduct could not be assigned. In this paper we have provided assignments for key resonances of the anthramycin–d(ATGCAT)$_2$ adduct, which allows for an analysis of the

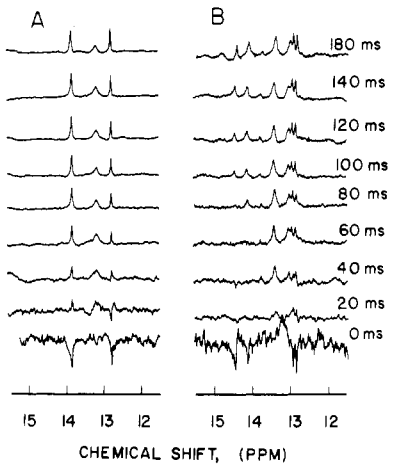

FIGURE 10: Nonselective spin–lattice relaxation experiments (5 mM concentration in H_2O, 15 °C). Shown are the imino protons of (A) the d(ATGCAT)$_2$ duplex and (B) the anthramycin–d(ATGCAT)$_2$ adduct. Delay times (τ) range from 0 to 180 ms. Spectra were obtained by using inversion recovery and water suppression techniques as discussed in the text.

dynamics and conformation of the adduct.

Effects of Anthramycin on the Thermal Stability and Dynamics of d(ATGCAT)$_2$. The stability of the DNA duplex may be monitored by the melting behavior of the imino protons, and by their relaxation rates. The imino protons are involved in the formation of the Watson–Crick hydrogen bonds between bases and are thus sensitive to breathing, fraying, and helical distortions of the duplex. In the free d(ATGCAT)$_2$ duplex, melting has been shown to proceed from the terminal (base pair fraying) toward the central G·C as the temperature is increased (Patel, 1975). At 20 °C, all of the imino resonances of the hexamer broaden into the base line due to rapid exchange with solvent. Formation of the anthramycin–d(ATGCAT)$_2$ adduct results in the increased thermal stability of the duplex, as illustrated by the persistence of the imino protons up to temperatures of 40 °C for the internal A^{11}·T^2 and 50 °C for the two G·C imino protons, respectively (Graves et al., 1984).

The temperature dependence of the T_1 relaxation rates of imino protons for a dodecamer was investigated by Early et al. (1981). They noted that for deoxyoligonucleotides of this size, the overall tumbling of the molecule dominates the effects of internal motion on the relaxation process. At temperatures significantly below the T_m, relaxation of the imino protons is controlled by dipole–dipole interactions. At higher temperatures, however, exchange with solvent becomes the dominant mechanism of relaxation.

The line widths of the imino resonances of d(ATGCAT)$_2$ (Figure 10A) suggest that solvent exchange makes a significant contribution to the relaxation of the imino resonances. In comparing the T_1 values for the imino protons of d(ATGCAT)$_2$ and the anthramycin–d(ATGCAT)$_2$ adduct, we note that the T_1's for the internal A·T imino protons are significantly longer in the adduct, which suggests that anthramycin binding stabilizes the internal A·T base pairs (A^{11}·T^2 and A^5·T^8) with respect to solvent exchange. The A^{11}·T^2 base pair exhibits the greatest thermal stability of the four A·T base pairs in the adduct (Graves et al., 1984), which may result from hydrogen bond formation between the anthramycin amide group and the 2-carbonyl group of T^2, as suggested by inspection of CPK models. No changes in the T_1 values for the terminal A·T imino protons are observed in comparing d(ATGCAT)$_2$ and the anthramycin–d(ATGCAT)$_2$ adduct, suggesting that fraying of the terminal base pairs in the adduct

is substantial and that the dominant relaxation mechanism is proton exchange with the solvent.

The T_1 relaxation times of the base protons (with the exception of the adenine H_2 protons; see Table I) suggest that adduct formation alters significantly the tumbling motions of the duplex. The longer T_1 values for the nonexchangeable base protons indicate a longer correlation time for the adduct. If the overall rate of tumbling dominates T_1 relaxation (Early et al., 1981), then the longer correlation time for the adduct suggests a slower tumbling rate in solution. This is consistent with previous studies which suggested that anthramycin binding results in a stiffening of the DNA helix (Glaubiger et al., 1974).

Conformation of the Anthramycin–d(ATGCAT)$_2$ Adduct. The unmodified d(ATGCAT)$_2$ duplex is approximated by a B-DNA conformation, as evidenced by an analysis of COSY and NOESY data. In the anthramycin–d(ATGCAT)$_2$ adduct the NOESY cross-peaks that arise from vertical stacking interactions are present, which suggests that binding of anthramycin does not introduce substantial changes in the stacking of the bases in the deoxyoligonucleotide. The increased thermal stability of the adduct as compared to the unmodified duplex also is consistent with the maintenance of the base stacking of the duplex.

The formation of an aminal linkage between the anthramycin and the guanine amino group locates the anthramycin in the minor groove. The analysis of the NMR data for the deoxyoligonucleotide provides direct evidence for the location and orientation of the anthramycin moiety in the minor groove.

Significant changes are observed in the deoxyribose region of the spectrum upon formation of the anthramycin–d(ATGCAT)$_2$ adduct. Inspection of this spectral region (Figures 6 and 7) indicates that several of the sugar resonances of the adduct experience substantial changes in their chemical shifts upon adduct formation. The largest shifts upfield are observed for several of the $H_{4'}$, $H_{5'}$, and $H_{5''}$ protons that are located adjacent to the minor groove of the hexamer. Although unequivocal assignments of these resonances were not obtained, inspection of CPK models shows that for the proposed orientation of anthramycin in the minor groove, the $A^{11}H_{4',5',5''}$ protons are predicted to be in close proximity to π-electron systems of the anthramycin, which is consistent with the observed changes in the chemical shifts.

The stereochemistry of the anthramycin at the C_{11a} position generates a right-handed twist about the long axis of the drug and is predicted to limit the orientation of the anthramycin to a single conformation within the B-DNA helix (Petrusek et al., 1981). The observation of a specific NOE cross-peak between the anthramycin methyl and the A^5H_2 proton (Figure 9) supports this proposal. If more than one orientation of the anthramycin molecule within the binding site were possible, then a cross-peak to the $A^{11}H_2$ and the anthramycin methyl would be predicted. From our data, only a single cross-peak to the A^5H_2 proton is observed. We note, however, that failure to observe an NOE cannot be construed as proof that the corresponding orientation does not exist, since other mechanisms of relaxation could be operating.

Overall, the data indicate that major perturbations to the deoxyoligonucleotide conformation are not present in the anthramycin–d(ATGCAT)$_2$ adduct and that anthramycin is bound within the minor groove of the duplex. Covalent attachment of the anthramycin stabilizes the DNA duplex, and the integrity of the helix structure is maintained. The anthramycin acrylamide side chain is oriented in the 5′ direction from the guanine NH_2 binding site. The "breathing" of the internal A·T base pairs is lessened in the presence of the drug, and overall tumbling rate of the adduct in solution is reduced as compared to free d(ATGCAT)$_2$. Our data are consistent with the proposed model in which anthramycin is inserted into the minor groove in the orientation depicted in Figure 1D and provide new and affirmative evidence in favor of the model proposed by Hurley & Petrusek (1979) and Petrusek et al. (1981).

Acknowledgments

We wish to thank Dr. Laurence H. Hurley for the generous gift of anthramycin methyl ether, for supplying the stereo drawing of the anthramycin–d(ATGCAT)$_2$ adduct, and for helpful discussions concerning the molecular model of the adduct.

Supplementary Material Available

A figure and a description of the assignments of the deoxyribose $H_{1'}$ protons of d(ATGCAT)$_2$ determined from NOESY and COSY data and a figure showing an expansion of the aromatic region of the COSY spectrum of the anthramycin–d(ATGCAT)$_2$ adduct, providing assignments for several anthramycin protons (5 pages). Ordering information is given on any current masthead page.

References

Borer, P. N., Zanatta, N., Holak, T. A., Levy, G. C., van Boom, J. H., & Wang, A. H.-J. (1984) *J. Biomol. Struct. Dyn. 1*, 1373–1386.

Breslauer, K. (1981) *Biophys. Chem. 13*, 141–149.

Chou, S.-H., Hare, D. R., Wemmer, D. E., & Reid, B. R. (1983) *Biochemistry 22*, 3037–3041.

Early, T. A., Kearns, D. R., Hillen, W., & Wells, R. D. (1981) *Biochemistry 20*, 3756–3764.

Feigon, J., Denny, W. A., Leupin, W., & Kearns, D. R. (1983) *Biochemistry 22*, 5930–5942.

Glaubiger, D., Kohn, K. W., & Charney, E. (1974) *Biochim. Biophys. Acta 361*, 303–311.

Graves, D. E., Pattaroni, C., Krishnan, B. S., Ostrander, J. M., Hurley, L. H. & Krugh, T. R. (1984) *J. Biol. Chem. 259*, 8202–8209.

Haasnoot, C. A. G. (1983) *J. Magn. Reson. 52*, 153–158.

Haasnoot, C. A. G., & Hilbers, C. W. (1983) *Biopolymers 22*, 1259–1266.

Haasnoot, C. A. G., Westerink, H. P., van der Marel, G. A., & van Boom, J. H. (1983) *J. Biol. Struct. Dyn. 1*, 131–149.

Hare, D. R., Wemmer, D. E., Chou, S.-H., Drobny, G., & Reid, B. R. (1983) *J. Mol. Biol. 171*, 319–336.

Hilbers, C. W., & Patel, D. J. (1975) *Biochemistry 14*, 2656–2660.

Horwitz, S. B., Chang, S. C., Grollman, A. P., & Borkovec, A. B. (1971) *Science (Washington, D.C.) 174*, 159–161.

Hurley, L. H., & Petrusek, R. L. (1979) *Nature (London) 282*, 529–531.

Hurley, L. H., Allen, C. S., Feola, J. M., & Lubawy, W. C. (1979) *Cancer Res. 39*, 3134–3140.

Kohn, K. W., & Spears, C. L. (1970) *J. Mol. Biol. 51*, 551–572.

Kohn, K. W., Bono, V. H., Jr., & Kann, H. E., Jr. (1968) *Biochim. Biophys. Acta 155*, 121–129.

Kohn, K. W., Glaubiger, D., & Spears, C. L. (1974) *Biochim. Biophys. Acta 361*, 288–302.

Lee, C. H., & Tinoco, I., Jr. (1980) *Biophys. Chem. 11*, 283–294.

Leimgruber, W., Batcho, A. D., & Schenker, F. (1965) *J. Am. Chem. Soc. 87*, 5791–5795.

Mostad, A., Romming, C., & Storm, B. (1978) *Acta Chem. Scand., Ser. B 32*, 639–645.
Neumann, J. M., Huynh-Dinh, T., Kan, S. K., Genissel, B., Igolen, J., & Tran-Dinh, S. (1982) *Eur. J. Biochem. 124*, 317–323.
Patel, D. J. (1974) *Biochemistry 13*, 2396–2402.
Patel, D. J. (1975) *Biochemistry 14*, 3874–3898.
Patel, D. J., & Tonelli, A. E. (1975) *Biochemistry 14*, 3990–3996.
Petrusek, R. L., Anderson, G. L., Garner, T. F. Fannin, Q. L., Kaplan, D. J., Zimmer, S. G., & Hurley, L. H. (1981) *Biochemistry 20*, 1111–1119.
Stefanovic, V. (1968) *Biochem. Pharmacol. 17*, 315–323.
Tran-Dinh, S., Neumann, J. M., Huynh-Dinh, T., Genissel, B., Igolen, J., & Kan, S. K. (1982) *Org. Magn. Reson. 18*, 148–152.
Weiss, M. A., Patel, D. J., Sauer, R. T., & Karplus, M. (1984) *Nucleic Acids Res. 12*, 4035–4047.
Young, M. A., & Krugh, T. R. (1975) *Biochemistry 14*, 4841–4847.

Ciliary Dynein Conformational Changes As Evidenced by the Extrinsic Fluorescent Probe 8-Anilino-1-naphthalenesulfonate†

Andrea C. Saucier, Sabina Mariotti,‡ Susan A. Anderson, and Daniel L. Purich*,‡
Department of Chemistry, University of California, Santa Barbara, California 93106
Received October 26, 1984; Revised Manuscript Received April 15, 1985

ABSTRACT: The binding of 8-anilino-1-naphthalenesulfonate (ANS) to ciliary dynein ATPase leads to a marked increase in the dye's fluorescence intensity, accompanied by a blue shift in the observed fluorescence emission maximum. We found that dynein has 37 ± 3 ANS binding sites and that experimentally applied ANS concentrations failed to alter enzyme activity. The fluorescence properties of the enzyme–dye complex were used to learn more about the binding characteristics of dynein substrates and effectors and to probe for possible conformational changes of the enzyme. The fluorescence of the dynein–ANS complex is increased by a number of substrates, including ATP, GTP, and UTP. The transfer of excitation energy from dynein chromophores to adsorbed ANS was also investigated. Our findings indicate that dynein appears to undergo a localized conformational change in its interaction with ATP. Native dynein was also found to be conformationally different from heat-activated or NEM-modified enzyme as evidenced by the emission and excitation spectra of the various enzyme–ANS complexes.

For a number of protein systems, the fluorescent dye 8-anilino-1-naphthalenesulfonate has been used successfully as a probe in the investigation of hydrophobic regions and conformational changes. ANS[1] as a probe of protein hydrophobic sites was suggested by Stryer (1965), who studied its binding to apomyoglobin and apohemoglobin. In some instances, the binding of the ANS occurs at specific sites on the protein. Thus, for bovine serum albumin, the ANS may bind at the fatty acid binding site (Brand, 1970); for transaldolase, it may bind at the fructose 6-phosphate site (Daniel & Weber, 1966); for apohemoglobin and apomyoglobin, it may bind at the heme site (Stryer, 1965). An alternative use of the dye is to investigate the effector–protein interactions that may be associated with the changes in the fluorescence of the protein–ANS complex (Bloxham, 1973; Cheung, 1969). For example, several studies have reported the use of ANS binding to monitor glutamate dehydrogenase conformational changes (Thompson, 1967). The utility of ANS for studying the conformational state of myosin has been demonstrated in several reports, particularly that by Cheung & Morales (1969). They demonstrated that the fluorescence of myosin was quenched by its interaction with ANS and that this quenching resulted from a transfer of the excitation energy from myosin chromophores to the absorbed dye. They also found that this quenching was influenced by chemical modification of the enzyme; indeed, the decrease in transfer of excitation energy was attributed to changes in myosin conformation resulting from the amino acid side-chain modifications.

Dynein conformational changes at the active sites or at the location of dynein–microtubule interactions are important because such changes might relate to the origin of mechanical thrust in cell motility. Yet, virtually nothing is known about these anticipated conformational changes, and we investigated the fluorescent properties of the ciliary dynein ATPase interactions with ANS. As will be reported below, we found that dynein ATPase displays a large number of ANS binding sites, and this is an unlikely property for ANS binding strictly at the nucleotide hydrolytic site. The fluorescent properties of the complex appear to be a useful indicator of conformational changes that may be induced in the protein by different substrates and/or effectors of the enzyme. The transfer of excitation energy from dynein chromophores to the adsorbed ANS was also investigated. Because transfer of excitation energy results from dipolar interactions, transfer efficiency is

† This work has been supported in part by NIH Research Grant GM-24958 from the U.S. Public Health Service.
‡ Present address: Department of Biochemistry and Molecular Biology, J. H. Miller Health Center, College of Medicine, University of Florida, Gainesville, FL 32610.

[1] Abbreviations: ANS, 8-anilino-1-naphthalenesulfonate magnesium salt; EHNA, *erythro*-9-(2-hydroxy-3-nonyl)adenine; NEM, *N*-ethylmaleimide; Hepes, *N*-(2-hydroxyethyl)piperazine-*N*′-2-ethanesulfonic acid; Tris, tris(hydroxymethyl)aminomethane; PMSF, phenylmethanesulfonyl fluoride; PEP, phosphoenolpyruvate; ATPγS, adenosine 5′-*O*-(3-thiotriphosphate); AMPPCH$_2$P, adenosine 5′-(β,γ-methylenetriphosphate).

0006-2960/85/0424-7581$01.50/0